JOURNAL OF GUIDANCE, CONTROL, AND DYNAMICS
Vol. 18, No. 1, January–February 1995

Fundamental Mechanisms of Aeroelastic Control with Control Surface and Strain Actuation

Kenneth B. Lazarus,* Edward F. Crawley,† and Charrissa Y. Lin‡
Massachusetts Institute of Technology, Cambridge, Massachusetts 02139

A typical section analysis is employed to provide an understanding of the fundamental mechanisms and limitations involved in performing aeroelastic control. The effects of both articulated aerodynamic control surfaces and induced strain actuators are included in the model. The ability of these actuators to effect aeroelastic control is studied for each actuator individually as well as in various combinations. The control options available are examined for single-input, single-output (SISO) and multiple-input, multiple-output (MIMO) classical and optimal control laws. A state-cost-vs-control-cost analysis is performed to assess the effectiveness of optimal linear quadratic regulator (LQR) control laws for different actuators and actuator combinations. The cost comparisons show that strain actuation is an effective means of achieving aeroelastic control and a viable alternative to articulated control surface methods. In addition, the advantages of using multiple actuators to avoid limitations associated with single-actuator systems are demonstrated.

Introduction

IN order to enhance aircraft performance and ride quality, it is desirable to control the lifting surfaces of aircraft using active aeroelastic control. Several options exist for implementing aeroelastic control schemes. Aeroelastic control may be effected by altering the lifting forces acting on the wing through articulation of leading- or trailing-edge control surfaces. Control may also be effected by induced strain actuators, such as piezoceramics and electrostrictives, which directly deform the structure through electromechanical coupling terms that appear in the actuator constitutive relations.

A great deal of research has been performed over the past few decades concerning the development and implementation of various feedback control schemes that utilize articulated actuator systems. Researchers have examined the fundamentals of traditional aeroservoelasticity using typical section models, simplified aerodynamics, and classical control methods.[1,2] More representative models and modern control techniques have been applied to examine such problems as flutter suppression[3–5] and gust alleviation.[6] In addition, topics such as model order reduction,[7,8] multiple control surface actuation,[9] and aeroservoelastic tailoring optimization[10] have been studied.

In contrast to the above work, this paper also examines the use of an alternative method of actuation. This technique involves the use of induced strain actuators, which are regulated to apply forces and moments on the lifting surface, in order to deform the wing and effect dynamic aeroelastic control. Recently, induced strain actuation has been shown to be effective for the static control of flexible lifting surfaces. Earlier investigations identified the parameters involved in effecting static aeroelastic control with strain actuators,[11] examined the use of strain actuators in conjunction with tailored composites,[12] and demonstrated the static control effectiveness of strain actuation for representative lifting surfaces.[13]

The actuator or combination of actuators selected has a direct bearing on the effectiveness of the control system. Equally as important is the choice of sensors and output variables measured and fed back to the controller. In order to choose the best combination of actuators and sensors for a particular lifting surface, it is essential to understand the fundamental mechanisms involved in aeroelastic control and the advantages and inherent limitations of such control systems. The objective of this study therefore is to explore the fundamental elements involved in controlling dynamic aeroelastic systems and to develop a method for consistently comparing various control schemes in order to assess the advantages and limitations of each. In order to gain an understanding of the basic physical aspects involved in dynamic aeroelastic control, a two-degree-of-freedom typical section is employed. The forces and moments produced by both induced strain actuators and conventional articulated control surfaces are included in the typical section model.

In this paper, the governing equations for the typical section with induced strain and conventional actuators are derived. The plant dynamics are examined, as are the feedback schemes associated with the various possible state outputs and various possible control inputs for several types of control laws. Control schemes are developed for single-input, single-output (SISO) and full state feedback multiple-input, multiple-output (MIMO) systems using both classical and modern state-space techniques. These control laws are compared and a closed-loop state-vs-control-cost analysis is performed for various input combinations using solutions to the linear quadratic regulator (LQR) problem. The analysis reveals the fundamental benefits and limitations of employing various control schemes for aeroelastic control. The results obtained can be applied to a wide variety of aeroservoelastic problems, such as flutter, vibration suppression, gust alleviation, and low-frequency servo shape control for maneuverability.

Typical Section Governing Equations

For many years, low-order models called typical sections have been used to explain the fundamental mechanics of aeroelasticity.[14] These sections capture the essential physical features and have properties representative of actual lifting surfaces. The geometry of the typical section employed in this analysis is shown in Fig. 1. The section is given plunge $\bar{h}$ and pitch α degrees of freedom and a leading- and trailing-edge flap. The structural restraints in bending and torsion appear at the elastic axis, and the disturbance to the section is a time variation in the angle of attack α_0.

The aerodynamics are found by adapting the incompressible wing-aileron-tablifting surface results obtained by Theodorsen and Garrick[15] to a leading-edge flap-wing-trailing-edge flap lifting surface via a coordinate transformation. Only the steady-state aerodynamic terms are retained to simplify the initial examination of the problem. A subsequent study incorporating unsteady aerodynamic loads shows that the same fundamental principles hold whether steady or unsteady aerodynamics are assumed.[16] The aerodynamic

Received April 6, 1992; revision received May 19, 1994; accepted for publication May 19, 1994.

*Graduate Research Assistant, Space Engineering Research Center. Member AIAA.

†Professor of Aeronautics and Astronautics, Space Engineering Research Center. Fellow AIAA.

‡Graduate Research Assistant, Space Engineering Research Center. Student Member AIAA.

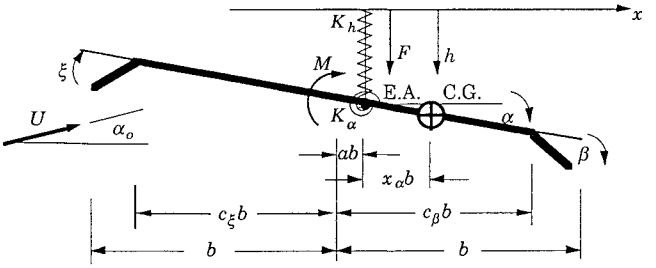

Fig. 1 Typical section geometry with leading- and trailing-edge flaps.

forces and moments created by deflecting the leading-edge ξ or trailing-edge β flap are modeled as forces and moments acting at the elastic axis, so that the high-frequency dynamics associated with the flaps can be neglected. The typical section also includes a force F and a moment M acting at the elastic axis that result from commands to the strain actuators. These are the equivalent forces and moments acting on the typical section that develop as a result of induced strain actuation. The equivalent forces and moments are found by applying Bernoulli-Euler beam and Kirchhoff plate theory as done in Crawley and de Luis[17] or Crawley and Lazarus.[11]

Writing the equations in terms of nondimensional mass $\boldsymbol{M}$, stiffness $\boldsymbol{K}$, forcing $\boldsymbol{f}$, and disturbance $\boldsymbol{d}$ matrices in the normalized Laplace domain p yields

$$\boldsymbol{M}\begin{Bmatrix}\bar{h}p^2\\ \alpha p^2\end{Bmatrix}+\boldsymbol{K}\begin{Bmatrix}\bar{h}\\ \alpha\end{Bmatrix}=\boldsymbol{f}\begin{Bmatrix}u_h\\ u_\alpha\\ u_\beta\\ u_\xi\end{Bmatrix}+\boldsymbol{d}\alpha_0(p) \tag{1a}$$

or

$$\begin{bmatrix}\frac{1}{R_\alpha^2} & \frac{x_\alpha}{R_\alpha^2}\\ \frac{x_\alpha}{R_\alpha^2} & 1\end{bmatrix}\begin{Bmatrix}\bar{h}p^2\\ \alpha p^2\end{Bmatrix}+\begin{bmatrix}\frac{\bar{\omega}_h^2}{R_\alpha^2} & \bar{q}C_{L_\alpha}\\ 0 & 1-\bar{q}C_{M_\alpha}\end{bmatrix}\begin{Bmatrix}\bar{h}\\ \alpha\end{Bmatrix}$$

$$=\begin{bmatrix}1 & 0 & -\bar{q}C_{L_\beta} & -\bar{q}C_{L_\xi}\\ 0 & 1 & \bar{q}C_{M_\beta} & \bar{q}C_{M_\xi}\end{bmatrix}\begin{Bmatrix}u_h\\ u_\alpha\\ u_\beta\\ u_\xi\end{Bmatrix}+\begin{bmatrix}-\bar{q}C_{L_\alpha}\\ \bar{q}C_{M_\alpha}\end{bmatrix}\alpha_0 \tag{1b}$$

where

$\bar{q}$ = normalized dynamic pressure, $U_\alpha^2/\pi\mu R_\alpha^2$
p = normalized Laplace variable, λ/ω_α
u_h = normalized strain-actuated plunge force, Fb/K_α
u_α = normalized strain-actuated pitch torque, M/K_α
u_β = trailing-edge flap deflection, β
u_ξ = leading-edge flap deflection, ξ

and the remaining nondimensional variables are those usually employed in a typical section analysis.[14] Note that the equivalent force u_h and moment u_α produced by the induced strain actuators are normalized by the section torsional stiffness.

The characteristic equation for this two-degree-of-freedom system is found by setting the right-hand side of Eq. (1) equal to zero:

$$\Delta(p)=\left(1-\frac{x_\alpha^2}{R_\alpha^2}\right)p^4+\left[\left(\bar{\omega}_h^2+1\right)-\bar{q}\left(C_{L_\alpha}x_\alpha+C_{M_\alpha}\right)\right]p^2$$
$$+\left[\bar{\omega}_h^2\left(1-\bar{q}C_{M_\alpha}\right)\right] \tag{2}$$

Equation (2) shows that the roots of the system (i.e., transfer function poles) are dependent on the section geometry, structural properties, and air speed but are independent of the actuation method. Note that there is no structural or air damping modeled in the system.

The transfer functions from the four control inputs (bending strain actuation u_h, torsion strain actuation u_α, trailing-edge flap deflection u_β, and leading-edge flap deflection u_ξ) to the two output variables (plunge $\bar{h}$ and pitch α) are given by

$$\begin{Bmatrix}\bar{h}\\ \alpha\end{Bmatrix}=\frac{R_\alpha^2}{\Delta(p)}\begin{bmatrix}n(p)_{hh} & n(p)_{h\alpha} & n(p)_{h\beta} & n(p)_{h\xi}\\ n(p)_{\alpha h} & n(p)_{\alpha\alpha} & n(p)_{\alpha\beta} & n(p)_{\alpha\xi}\end{bmatrix}\begin{Bmatrix}u_h\\ u_\alpha\\ u_\beta\\ u_\xi\end{Bmatrix}$$

$$n(p)_{hh}=p^2+1-\bar{q}C_{M_\alpha}$$

$$n(p)_{\alpha h}=-\frac{x_\alpha p^2}{R_\alpha^2}$$

$$n(p)_{h\alpha}=-\frac{x_\alpha p^2}{R_\alpha^2}-\bar{q}C_{L_\alpha}$$

$$n(p)_{\alpha\alpha}=\frac{p^2}{R_\alpha^2}+\frac{\bar{\omega}_h^2}{R_\alpha^2}$$

$$n(p)_{h\beta}=\bar{q}C_{L_\beta}\left[\bar{q}C_{M_\alpha}\left(1-\frac{C_{L_\alpha}C_{M_\beta}}{C_{M_\alpha}C_{L_\beta}}\right)-1\right. \tag{3}$$
$$\left.-p^2\left(1+\frac{C_{M_\beta}x_\alpha}{C_{L_\beta}R_\alpha^2}\right)\right]$$

$$n(p)_{\alpha\beta}=\frac{1}{R_\alpha^2}\bar{q}C_{M_\beta}\left[p^2\left(1+\frac{C_{L_\beta}x_\alpha}{C_{M_\beta}}\right)+\bar{\omega}_h^2\right]$$

$$n(p)_{h\xi}=\bar{q}C_{L_\xi}\left[\bar{q}C_{M_\alpha}\left(1-\frac{C_{L_\alpha}C_{M_\xi}}{C_{M_\alpha}C_{L_\xi}}\right)-1\right.$$
$$\left.-p^2\left(1+\frac{C_{M_\xi}x_\alpha}{C_{L_\xi}R_\alpha^2}\right)\right]$$

$$n(p)_{\alpha\xi}=\frac{1}{R_\alpha^2}\bar{q}C_{M_\xi}\left[p^2\left(1+\frac{C_{L_\xi}x_\alpha}{C_{M_\xi}}\right)+\bar{\omega}_h^2\right]$$

where each element $n_{ij}(p)$ of this 2×4 matrix relation represents the transfer function from one of the inputs to one of the outputs. The zeros of each individual SISO transfer function are found by setting each numerator $n_{ij}(p)$ to zero. The zero locations are dependent on the section geometry and structural properties, as were the system poles. For the case of plunge $\bar{h}$ measurement feedback, the individual SISO transfer function zeros move rapidly with air speed. For the case of pitch measurement α feedback, the zeros are not dependent on air speed.

Alternatively, the governing equations [Eq. (1)] can be written in a state-space representation as

$$\dot{\boldsymbol{x}}=\boldsymbol{A}\boldsymbol{x}+\boldsymbol{B}\boldsymbol{u}+\boldsymbol{L}\alpha_0(p) \qquad \boldsymbol{y}=\boldsymbol{C}\boldsymbol{x}$$
$$x=\begin{Bmatrix}\bar{h}\\ \alpha\\ \dot{\bar{h}}\\ \dot{\alpha}\end{Bmatrix} \qquad u=\begin{Bmatrix}u_h\\ u_\alpha\\ u_\beta\\ u_\xi\end{Bmatrix} \tag{4}$$

Typical Section Properties

As seen from Eqs. (2) and (3), the location of the system poles and transfer function zeros are highly dependent on the geometric and structural properties of the typical section. Therefore it is necessary to choose some nominal parameters in order to proceed with the analysis and control system design. The section properties chosen were those at the three-quarter span of the aluminum induced-strain-actuated test article described by Crawley and Lazarus.[11] The test article had a full span aspect ratio of 3.9 and a thickness-to-chord ratio of about 0.51%. The resulting typical section is altered to include 10% leading- and trailing-edge flaps; the elastic axis is moved forward of the midchord by 10% of the chord so that flutter occurs before static divergence. The resulting typical section has a frequency ratio $\bar{\omega}_h$ of 0.2 and a mass ratio μ of 20. Other relevant section properties are listed in Table 1.

Table 1 Nominal geometric and material properties of the typical section

Parameter	Symbol	Value
Section geometry	a	-0.2
	x_α	0.2
	R_α^2	0.25
	μ	20
	$\bar{\omega}_h$	0.2
Wing parameters	$t/2b$	0.51%
	L/b	3.92
Steady aerodynamics coefficients	C_{L_α}	2π
	C_{M_α}	1.885
	C_{L_β}	2.487
	C_{M_β}	-0.334
	C_{L_ξ}	-0.087
	C_{M_ξ}	-0.146
State cost matrix	N_{hh}	$(1/0.406)^2$
	$N_{\alpha\alpha}$	$(1/0.282)^2$
Control cost matrix	R_{hh}	$(1/0.0429)^2$
	$R_{\alpha\alpha}$	$(1/0.0215)^2$
	$R_{\beta\beta}$	$(1/0.0873)^2$
	$R_{\xi\xi}$	$(1/0.0436)^2$

Knowledge of the system pole and zero locations is important for determining the manner in which a system can be controlled and is essential in designing SISO feedback control laws. In aeroelastic systems, all of the pole and some of the zero locations are a function of air speed U_α, which indicates that a control law appropriate at one flight condition may not necessarily be appropriate at others. The rate of zero movement and the propensity for the pole/zero pattern along the imaginary axis to change (i.e., pole/zero flipping) is a particular indicator of the potential nonrobustness of the closed-loop control scheme.[18] It is therefore interesting to observe the relative and absolute movement of the system poles and the SISO transfer function zeros as a function of air speed. Such a plot of the purely oscillatory poles and zeros associated with plunge measurement feedback is shown in Fig. 2. Notice the two poles coalesce at the flutter point ($U_\alpha = 1.90$).

For the case of plunge $\bar{h}$ measurement feedback, all four of the individual SISO transfer function zeros change with wind speed. The SISO transfer function zeros associated with the bending strain actuator u_h are at the torsional natural frequency ω_α when the air speed is zero. These zeros decrease quadratically to zero at the divergence speed ($U_\alpha = 2.88$). Likewise, the zeros associated with the trailing-edge flap actuator u_β decrease quadratically with wind speed to zero at the reversal speed ($U_\alpha = 2.40$). The air speed at which the frequency component of the individual SISO transfer function zeros goes to zero is especially significant in the aeroelastic control problem, since it is at this air speed that one of the zeros becomes non–minimum phase (i.e., moves into the right half of the Laplace plane). The presence of a non-minimum-phase zero indicates a fundamental limitation on the amount of control that can be applied to the system.[19] The zeros associated with the torsion strain actuator u_α and leading-edge flap actuator u_ξ also move with air speed. The zeros in both of these SISO transfer functions increase with air speed, as shown in Fig. 2.

The individual SISO transfer function zeros associated with pitch α measurement feedback, which are independent of the air speed, are not shown in Fig. 2. Examining Eq. (3), it can be seen that the two zeros associated with the bending strain actuator u_h are always at the origin and that the two zeros associated with the torsion strain actuator u_α are always on the imaginary axis at $\bar{\omega}_h$. In both cases this places the zeros below the lower (plunge) pole of the system for all nonzero air speeds. The zeros associated with the leading-edge flap u_ξ and trailing-edge flap u_β actuators depend on $\bar{\omega}_h$ and the aerodynamic influence coefficients and may be imaginary or real. In the event they are real, once again one would be a non-minimum-phase zero, indicating a limitation on achievable control.

Because of the significant movement of the system poles and zeros as a function of air speed, it is necessary to choose specific dynamic pressures to analyze the system and design feedback control schemes. Two air speeds are chosen and are indicated on the pole locus plot in Fig. 3. The first speed is at about 10% below the flutter velocity and is designated as design point 1($U_\alpha = 1.71$). The second is chosen at about 5% above the flutter velocity and is designated as design point 2($U_\alpha = 2.00$). Both design points are below reversal and divergence. These speeds are chosen so that the control law designs are dominated by fundamental aeroelastic control issues and are not complicated by factors such as aileron reversal or static instabilities.

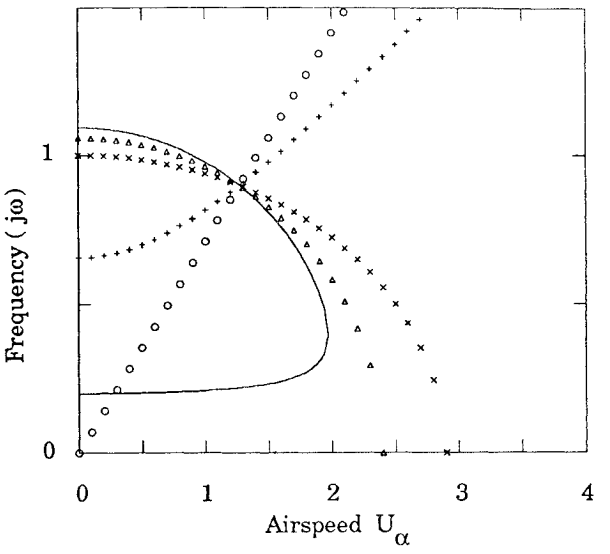

Fig. 2 Pole and individual SISO transfer function zero frequencies for plunge measurement vs air speed U_α. —— system poles, × bending strain control/plunge output, ○ torsion strain control/plunge output, △ trailing edge flap control/plunge output, + leading edge flap control/plunge output.

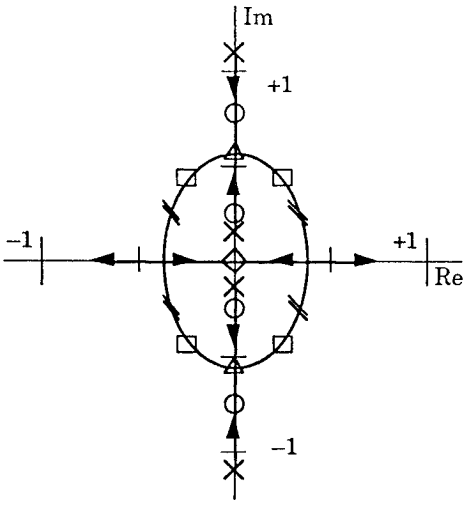

Fig. 3 Location of open-loop poles as function of nondimensional air speed U_α. × Zero air speed poles, $U_\alpha = 0.00$, ○ design point 1, $U_\alpha = 1.71$, △ flutter speed, $U_\alpha = 1.90$, □ design point 2, $U_\alpha = 2.00$, \\ reversal speed, $U_\alpha = 2.40$, ◇ divergence speed, $U_\alpha = 2.88$.

Single-Input, Single-Output Control

The combination of four actuator control inputs and two measurement output variables allows for eight SISO feedback control options to be considered. The transfer functions for the eight options are defined by Eq. (3), and the locations of the poles and zeros are illustrated graphically in Fig. 4 for the below-flutter design point ($U_\alpha = 1.71$). At this wind speed, all the poles lie on the imaginary axis, indicating that each system is neutrally stable. Thus, the control objective is to add damping to the modes of the system.[20] Note that in each system there is a zero "missing" from between the two poles (i.e., between the two system poles there is no zero). This missing zero dictates that simple gain feedback, either displacement

$u = -gz$ or rate $u = -pgz$, will not stabilize the system (i.e., add damping) for any value (or sign) of the gain g.

For the cases of pitch feedback to bending strain actuation α/u_h, pitch feedback to torsion strain actuation α/u_α, and pitch feedback to leading-edge flap actuation α/u_ξ the pitch mode can be stiffened (the frequency of this pole increases), but no damping is added to the closed-loop system (i.e., the poles do not move into the left half of the Laplace plane). In all other cases, the closed-loop system is destabilized (i.e., a system pole moves into the right half of the Laplace plane) by displacement or rate feedback. Note also that the pitch measurement to the trailing-edge flap actuator α/u_β transfer function, a common conventionally used SISO loop, has a non-minimum-phase zero at this air speed.

Since simple feedback does not produce stable closed-loop systems, other control schemes must be employed. The first option is to place a sensor at some desirable point on the section so that a stabilizing combination of the plunge and pitch output variables are fed back to the actuator. The sensor placement relation can be expressed as

$$y = \bar{h} + x_s\alpha$$

or

$$\boldsymbol{c} = [1 \quad x_s \quad 0 \quad 0] \tag{5}$$

in state-space form. If the sensor can be placed in a position x_s, which places an SISO transfer function zero between the open-loop poles, the system can be stabilized using rate feedback of the output variable y. Equations (3) and (5) can be combined to give equations for the four SISO transfer functions between any of the four control inputs and the output measurement y. Setting the numerator of each transfer function to zero gives an expression for each SISO transfer function zero. The sensor position x_s can then be found that yields the desired SISO transfer function zeros for each method of actuation. The sensor positions as a function of the desired zero locations for the four actuation schemes are

$$x_s = \frac{R_\alpha^2}{x_\alpha}\left(1 - \frac{\bar{q}C_{M_\alpha} - 1}{p^2}\right) \qquad \text{for} \qquad u_h \text{ control}$$

$$x_s = \frac{x_\alpha p^2 + \bar{q}C_{L_\alpha}R_\alpha^2}{p^2 + \bar{\omega}_h^2} \qquad \text{for} \qquad u_\alpha \text{ control}$$

$$x_s = \frac{p^2\left(C_{M_\beta}x_\alpha/C_{L_\beta}R_\alpha^2 + 1\right) + 1 - \bar{q}C_{M_\alpha}\left(1 - C_{M_\beta}C_{L_\alpha}/C_{L_\beta}C_{M_\alpha}\right)}{\left(1/R_\alpha^2\right)\left[p^2\left(C_{M_\beta}/C_{L_\beta} + x_\alpha\right) + \left(C_{M_\beta}/C_{L_\beta}\right)\bar{\omega}_h^2\right]} \qquad \text{for} \qquad u_\beta \text{ control}$$

$$x_s = \frac{p^2\left(C_{M_\xi}x_\alpha/C_{L_\xi}R_\alpha^2 + 1\right) + 1 - \bar{q}C_{M_\alpha}\left(1 - C_{M_\xi}C_{L_\alpha}/C_{L_\xi}C_{M_\alpha}\right)}{\left(1/R_\alpha^2\right)\left[p^2\left(C_{M_\xi}/C_{L_\xi} + x_\alpha\right) + \left(C_{M_\xi}/C_{L_\xi}\right)\bar{\omega}_h^2\right]} \qquad \text{for} \qquad u_\xi \text{ control} \tag{6}$$

By choosing x_s such that the zero is between the poles, a stable closed-loop system results, in principle, for rate feedback. However, sensor placement will not work for all configurations or choices of actuators in practice. This is because the sensor location needed for stable feedback is sometimes found to be physically off of the typical section. For example, using the nominal typical section (Table 1) and design point 1 (below-flutter) values, it is possible to find a stable sensor location for each method of actuation (although this causes a near pole-zero cancellation in the trailing-edge flap actuation case y/u_β). However, all of the stabilizing sensor locations are found to be physically well off of the section at design point 2. Also, notice in Eq. (6) that, if the desired zero locations are not complex-conjugate pairs, the sensor position calculated will not be a real number.

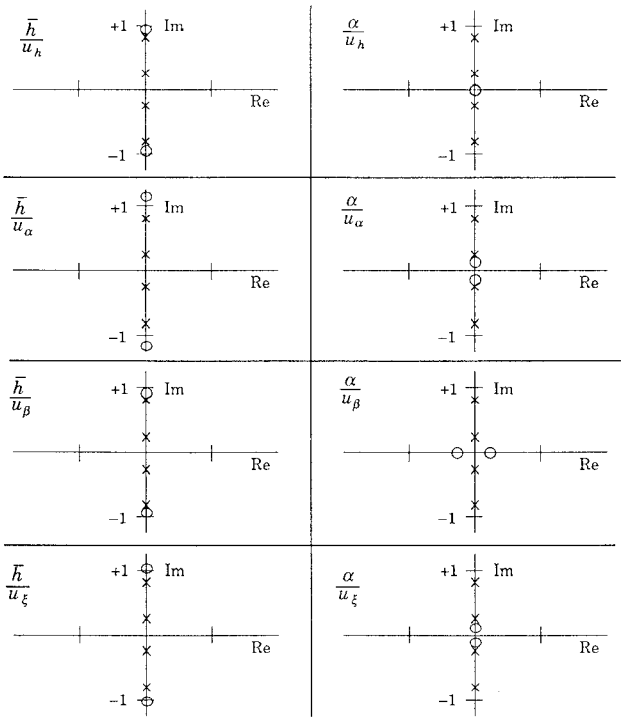

Fig. 4 Pole and zero locations for individual SISO input/output combinations at design point 1 ($U_\alpha = 1.71$).

Full State Feedback Control

The problems associated with non-physical sensor placement solutions can be eliminated by independently measuring the state variables and feeding back combinations of them that yield stable closed-loop systems. Using full state feedback is particularly advantageous because control laws may be developed that utilize various combinations of both the displacement and rate variables and are not limited to combinations corresponding to locations physically on the airfoil. Since full state feedback is not feasible in larger systems, the effects of using output feedback are examined in a subsequent analysis.[16] This analysis shows that the use of output feedback does not alter the qualitative results of this study.

The solution to the LQR problem generally provides for stable well-regulated closed-loop plants. Well-regulated closed-loop plants have the desirable properties of relatively high damping and good disturbance rejection, which satisfy the control objective of the systems under consideration (i.e., add damping). The optimal gains $\boldsymbol{G}$ for full state feedback can be found by solving the LQR problem, which entails minimizing the scalar cost functional J:

$$J = \int_0^\infty (\boldsymbol{x}^T\boldsymbol{Q}\boldsymbol{x} + \rho\boldsymbol{u}^T\boldsymbol{R}\boldsymbol{u})\,\mathrm{d}t \qquad \boldsymbol{Q} = \boldsymbol{N}^T\boldsymbol{N} \qquad \boldsymbol{z} = \boldsymbol{N}\boldsymbol{x} \tag{7}$$

In Eq. (7), $\boldsymbol{Q}$ is the penalty on the states and $\rho\boldsymbol{R}$ is the penalty on the control inputs that combines a scale factor ρ and an actuator weighting matrix $\boldsymbol{R}$. The feedback gains are given by $\boldsymbol{u} = -\boldsymbol{G}\boldsymbol{x}$. The gains represent the optimal combination of the states to be fed back to each actuator. Note that the LQR solution yields a loop transfer function, given by $\boldsymbol{G}\Phi\boldsymbol{B}$, which will always have the stable alternating pole-zero pattern (although the zeros may not be on the imaginary axis). This result holds for any air speed, state cost $\boldsymbol{N}$, or state control cost $\rho\boldsymbol{R}$.

An interesting result is found in the case of "expensive" control, which implies a large control penalty (ρ goes to infinity) and therefore small gains. An asymptotic analysis shows that the feedback gains are given by

$$g = \frac{1}{\sqrt{\rho}}\sum_i \sqrt{v_i^H\boldsymbol{Q}v_i}\,\frac{\left(w_i^H\boldsymbol{b}\right)^H}{\left|w_i^H\boldsymbol{b}\right|}w_i^H \tag{8}$$

where v_i and w_i are the right and left eigenvectors of $\boldsymbol{A}$ and the superscript H indicates the complex-conjugate transpose.

For single-control-input systems, $(w_i)^H \boldsymbol{b}$ is a scalar, so the entire quantity except for the last term w_i^H is a scalar. Therefore, the feedback gains are determined only by a weighted sum of the left eigenvectors of the open-loop system. The weights are given by the contribution of the modes (observability) to the state cost chosen. In the expensive control case the LQR solution produces gains that are nonzero only on the rate state variables. This result is true for any undamped single-input system. The gains on the rate variables represent the optimal combination of states to use for rate feedback, and thus the LQR solution is equivalent to a sophisticated rate feedback sensor placement algorithm (although the sensor does not have to be placed physically on the wing). In this low-gain case the LQR solution attempts only to add damping to the system. The results show once again that damping is best added to an initially undamped structure by feeding back a stabilizing combination of the rate states. As the control becomes less expensive (ρ decreases), some displacement feedback will also be added.

Although the LQR controller generally provides for stable well-regulated closed-loop systems, its performance has limitations. This is especially true for the single-control-input case. Such restrictions become most apparent in the limiting case of "cheap" control. Cheap control is associated with a small control penalty and high feedback gains. As the control weight ρ goes to zero, the closed-loop poles go to the stable finite MIMO zeros of the full Hamiltonian system if they exist,[21] or otherwise to infinity along stable Butterworth patterns. The MIMO zeros of the full Hamiltonian system are found by calculating the zeros of

$$\boldsymbol{H}(p) = [\boldsymbol{N}\Phi(-p)\boldsymbol{B}]^T[\boldsymbol{N}\Phi(p)\boldsymbol{B}] \tag{9}$$

These zeros are referred to as transmission zeros for square (number of measurements equals number of actuators) systems since they are the zeros of the MIMO loop transfer function $\boldsymbol{G}\Phi\boldsymbol{B}$. For nonsquare systems, these zeros include both transmission zeros and "compromise" zeros. Compromise zeros do not appear in the MIMO loop transfer function.

For any system, having fewer actuators than performance variables or important modes indicates a fundamental limit on the performance of the control system.[23] This limitation is clearly illustrated in Figs. 5 and 6, which show the movement of the LQR closed-loop pole locations of the nominal system at design point 1 (below flutter). The closed-loop poles are plotted for control weights that decrease from a large value toward zero (from $\rho = 10^4$ to $\rho = 10^{-4}$). As the control weight decreases, the calculated control gain increases, causing the poles to move away from their open-loop locations. In producing the pole loci of Figs. 5 and 6, the gains of the closed-loop systems are calculated using a state cost penalty that is an evenly weighted combination of the plunge and pitch output variables normalized by their maximum values. The maximum values (Table 1) are determined from the deflection associated with a quadratic bending or linear twist distribution in a beamlike wing and a maximum strain of 1%.

The pole locations are plotted in Fig. 5 for the cases of the four actuators acting individually. Figure 6 shows the closed-loop pole locations for the cases of the actuators acting in pairs (two inputs) and all controls acting together. When only one of the four available actuators is used, a compromise zero is found and only one pole is able to move along a stable Butterworth pattern. Such a zero, because it does not appear in the loop transfer function, indicates that a finite amount of state cost will persist, even when a large control effort is used. This point will be further illustrated by the state-vs-control-cost curves found in the following section. Notice that for the single-input cases the induced strain bending u_h and trailing-edge flap u_β actuators are able to move only the plunge pole along a stable Butterworth pattern. This indicates that these two actuators primarily influence the plunge mode. The induced strain torsion u_α and leading-edge flap u_ξ actuators are able to move only the pitch pole along a stable Butterworth pattern, indicating that these two actuators primarily influence the pitch mode. Also notice that the bending actuator is more effective than the trailing-edge flap actuator (i.e., the poles are moved farther into the left half of the

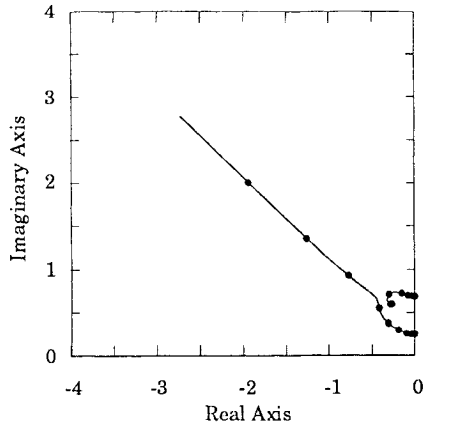

a) u_h control

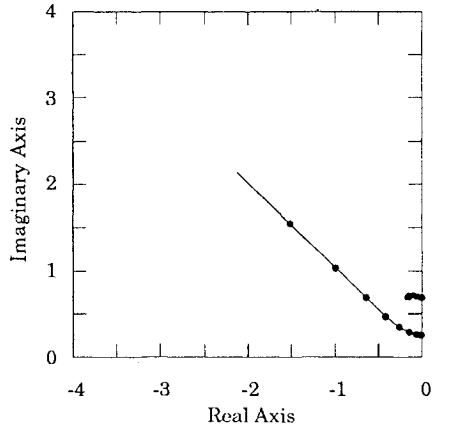

b) u_β control

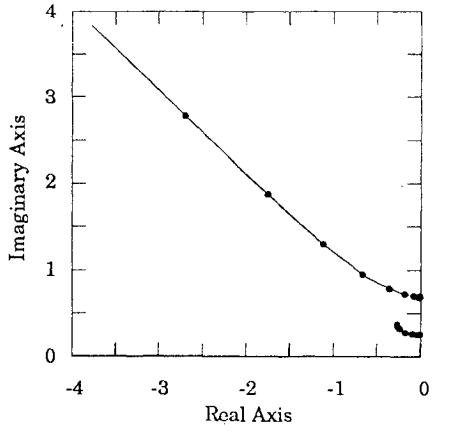

c) u_α control

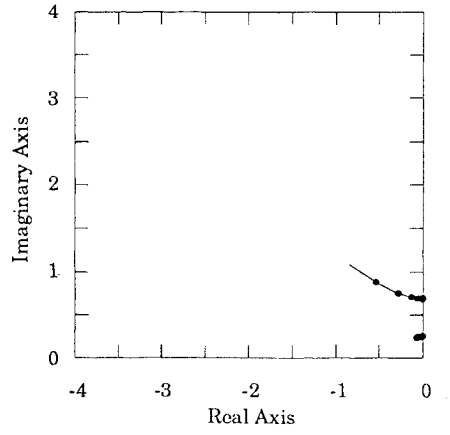

d) u_ξ control

Fig. 5 Locus of full state feedback LQR closed-loop poles as ρ goes toward zero (cheap control) for four actuators acting individually.

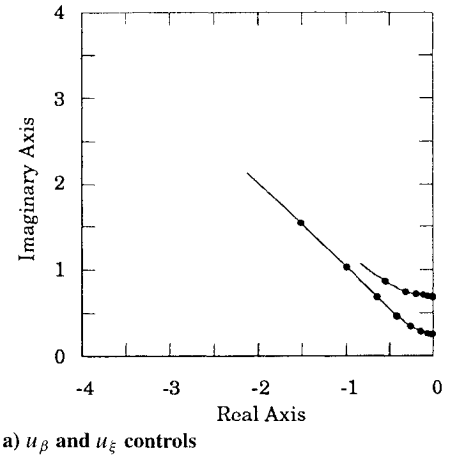

a) u_β and u_ξ controls

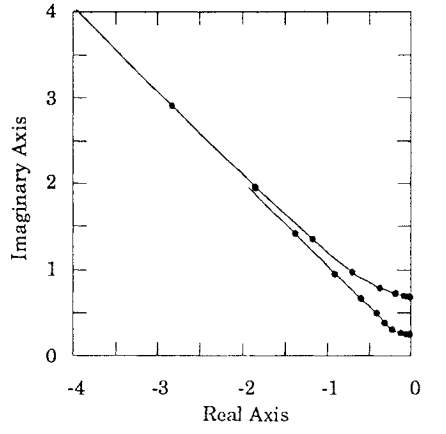

b) u_h and u_α controls

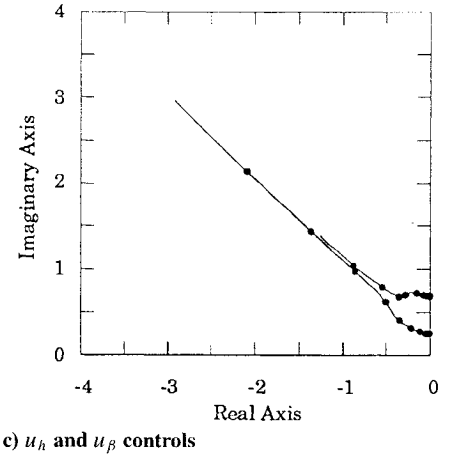

c) u_h and u_β controls

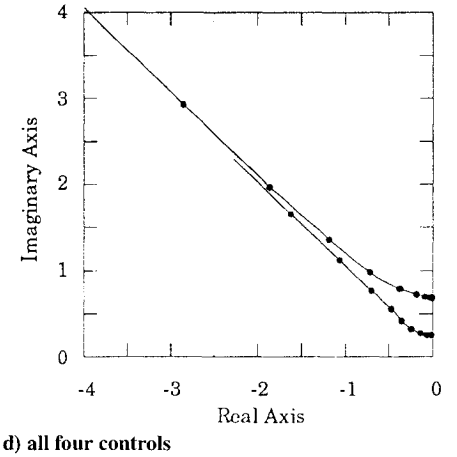

d) all four controls

Fig. 6 Locus of full state feedback LQR closed-loop poles as ρ goes to zero (cheap control) for multiple-actuator input configurations.

Laplace plane), and the torsion strain actuator is significantly more effective than the leading-edge flap actuator. In contrast with the single-actuator case, no compromise zeros are found when combinations of two or more actuators are used (Fig. 6). In these cases, both poles move along stable Butterworth patterns, although for a fixed ρ some combinations are clearly more effective than others.

State-Versus-Control-Cost Analysis

In order to qualitatively examine the effectiveness of the four actuators (bending strain actuation, torsion strain actuation, trailing-edge flap deflection, and leading-edge flap deflection) acting individually and in various combinations, several state-vs-control-cost analyses are performed. The nominal section properties are taken to be those found in Table 1, and the section is analyzed at design points 1 (below flutter) and 2 (above flutter). The feedback gains are found by solving the LQR problem with a state cost that equally penalizes the two normalized displacement states. These states are normalized by their maximum allowable deflection as before. Each of the controls is also normalized by its maximum value. For the strain actuators, the maximum control input is computed using a maximum actuation strain of $\Lambda = 600\ \mu\varepsilon$, which is considered a conservative value.[22] The maximum deflection for the trailing-edge flap is taken to be 5 deg, and the maximum leading-edge flap deflection is determined by equating its maximum hinge moment with that of the trailing-edge flap and is found to be about 2.5 deg. In order to determine a finite cost, a broadband disturbance source is introduced in the form of a 1 deg broadband variation of the free-stream airflow.

The results for design point 1 are shown in Figs. 7 and 8 in the form of state-cost-vs-control-cost curves. Each curve represents a different actuator configuration. In Fig. 7, curves are present for each actuator acting individually and all four acting together, the condition that creates the minimum state-vs-control-cost. In Fig. 8, the cost associated with combinations of any two actuators acting together are plotted as well as the curve for three actuators (bending strain, torsion strain, and trailing-edge flap) and of all four actuators acting together. The curves are derived by fixing all of the parameters of the problem except the control cost weighting ρ, which is varied from $\rho = 10^4$ to $\rho = 10^{-4}$. On these curves low control-cost values indicate expensive control weighting (high ρ), low gains, and therefore high state costs associated with large responses. High control-cost values indicate cheap control weighting (low ρ), high gains, and lower state costs associated with smaller responses. The lower the state cost for any given control cost, the greater the effectiveness of the actuator or combination of actuators.

As can be seen in Fig. 7 for single control inputs, the torsion strain control u_α is most effective in the low-gain expensive control case,

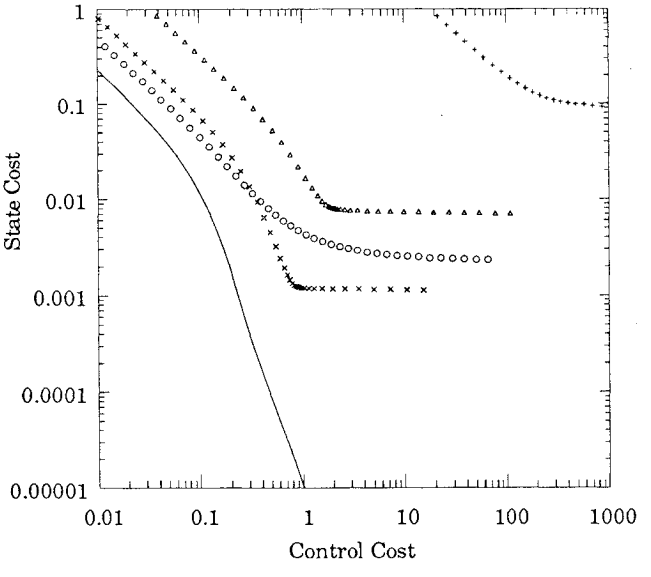

Fig. 7 State-vs-control cost at design point 1 (below flutter) for four actuators acting individually and all actuators acting together. × bending strain control, ○ torsion strain control, △ trailing edge flap control, + leading edge flap control, —— all four controls.

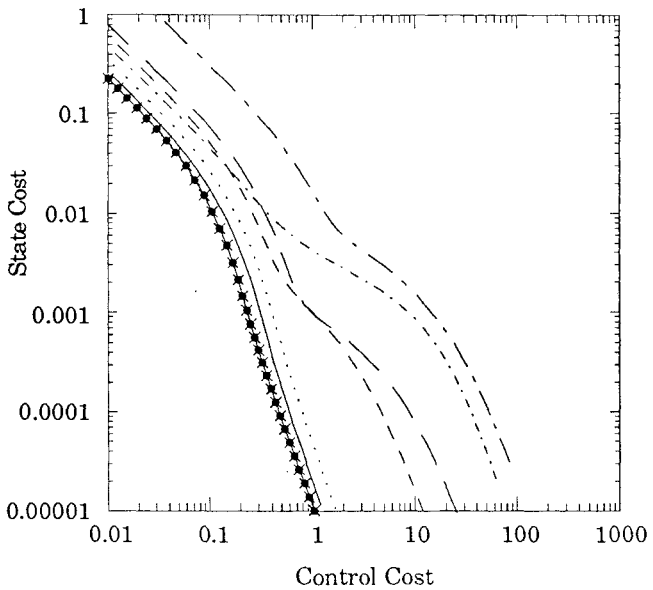

Fig. 8 State-vs-control cost at design point 1 (below flutter) for variety of multiple-input actuator combinations. — – leading edge flap and trailing edge flap controls, – · – torsion and leading edge flap controls, — — bending and leading edge flap controls, – – – bending trailing edge flap controls, · · · · · torsion and trailing edge flap controls, —— bending and torsion strain controls, —o— bending, torsion, and trailing edge flap controls, —×— all four controls.

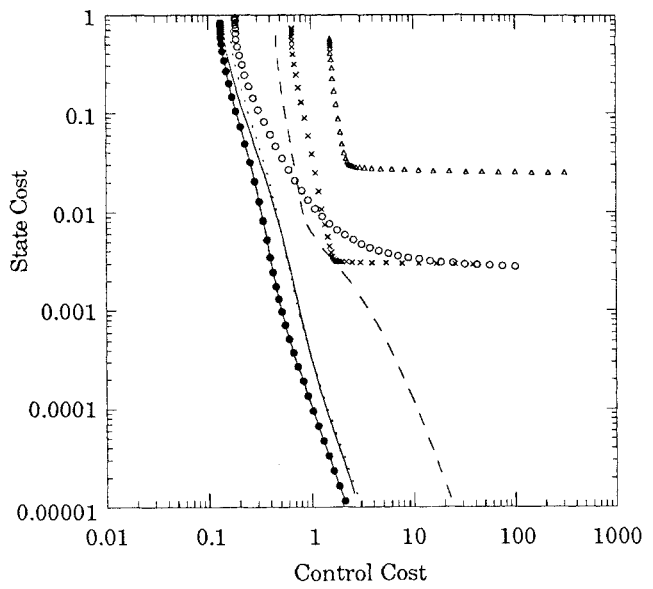

Fig. 9 State-vs-control cost at design point 2 (above flutter) for actuators acting individually and in multiple-input combinations. × bending strain control, o torsion strain control, △ trailing edge flap control, – – – bending and trailing edge flap controls, · · · · · torsion and trailing edge flap controls, —— bending and torsion strain controls, —o— bending, torsion and trailing edge flap controls.

whereas bending strain control u_h is most effective for high-gain cheap control. The cost curves show that the induced strain bending and torsion actuators are more effective than the conventional control surfaces throughout the entire range of control gains. It is also evident from the figure that the leading-edge control surface is significantly less effective than the other actuators. Each curve associated with a single control input is observed to flatten out or asymptote to some finite state cost value. It is at this point that each actuator reaches its fundamental limit in terms of ability to exert control on the system. Note that the actuators have *not* saturated but have imparted sufficient control to move one of the closed-loop poles asymptotically near an open-loop stable finite MIMO zero of the Hamiltonian system, as shown in Fig. 5. Since this closed-loop pole will move no further despite larger control effort, the state-vs-control-cost curve flattens. This is evidence of the fact that the presence of fewer independent actuators than important degrees of freedom in the system leads to compromise zeros[21] and places a fundamental limitation on the degree of control that can be exerted.[23]

The curves associated with control schemes that utilize more than one actuator are shown in Fig. 8 and are, in general, much more effective than the single-actuator systems.[24] This is especially true for the cheap control high-gain cases, where the improvement is observed to be over two orders of magnitude for some configurations. No fundamental performance limits are encountered in these multiple-input control systems for which the number of actuators (two or more) at least equals the number of degrees of freedom in the system. The state costs associated with the multiple-actuator systems are shown to decrease in Fig. 8 as the control effort is increased throughout the entire range of control gains. As the gains increase, the system closed-loop poles move outward along the stable Butterworth patterns, typified by the pairs shown in Fig. 6. The rate at which these poles move in the complex plane is directly related to the effectiveness of the multiple-actuator system in question.

Figure 8 shows that the combination of the bending and torsion strain actuators and the combination of the trailing edge flap and torsion strain actuators provide the best performance. These actuator combinations, bending and torsion strain or trailing-edge flap and torsion strain, are found to be effective because they combine an actuator that effectively controls plunge (bending strain or trailing-edge flap) with one that effectively controls torsion. In contrast, the bending strain and trailing-edge flap actuator combination is much less effective since both actuators tend to control only the bending force on the wing and have little influence on the torsional moment. Figure 8 also shows that the combination of "conventional" aerodynamic surfaces, leading-edge flap and trailing-edge flap, are the least effective actuator pair. In fact, all of the curves associated with the leading-edge flap exhibit poor performance. The pairs that include the leading-edge flap do not provide much more control performance than that given by the other actuators acting alone. The curves show that only after reaching the single-actuator asymptote does the presence of the leading-edge flap allow for more control to be effected. Finally, it is observed that the performance obtained using three actuators and all four actuators is only marginally better than that obtained using either the bending and torsion strain actuator combination or the trailing-edge flap and torsion strain actuator combination. This is because there are only two modes to be controlled and these two combinations of actuators can effectively control both modes. Therefore, little additional benefit is obtained when more actuators are used than modes important to the problem.

Figure 9 shows similar results for individual actuators and several combinations of actuators at design point 2 (above flutter). The strain actuators once again are more effective than the conventional control surfaces. The bending and torsion strain actuators are the most effective, whereas the leading-edge actuator provides only very small amounts of control and is not plotted in the figure. As with design point 1 (below flutter), actuator combinations are more effective than single-actuator control schemes, with the combination of bending and torsion strain actuation or torsion strain and trailing-edge flap actuation being most effective. Also notice the vertical low-gain asymptotes in Fig. 9. Unlike the systems in Figs. 7 and 8 (below flutter), which have finite state cost for infinitesimal gains, the systems of Fig. 9 (above flutter) are initially unstable, and the low-gain asymptotes shown in the figure are associated with the minimum amount of control required to stabilize each system.

Conclusions

A typical section model was analyzed to provide the tools necessary for understanding the fundamental mechanisms and limitations involved in aeroelastic control and for comparing alternative control methods. It was found that both the poles and zeros of the individual SISO transfer functions moved rapidly with air speed and that the zeros were often in undesirable locations for effecting SISO control, including being non–minimum phase. It was also found that simple gain feedback of the state variables would not stabilize the systems

considered and that it was necessary to use some combination of the rate states in order to achieve a stable feedback loop.

Stable feedback loops were found using sensor placement techniques and the solution to the LQR problem. For the limiting case of low-gain expensive control, the LQR solution was found to yield a solution similar to that of sensor placement but was not restricted to gain ratios that corresponded to physical sensor locations. To avoid the fundamental control limitations imposed by using fewer actuators than important modes, at least as many control actuators as important modes should be utilized.

The state-vs-control-cost comparisons demonstrated that strain actuation is an effective means of controlling aeroelastic systems and a viable alternative to conventional articulated control surfaces. Either bending or torsion strain actuation is as effective alone as trailing-edge flap actuation and much more effective than leading-edge flap actuation. Thus, only by incorporating strain actuation can an effective second actuator be added to the system and true high-gain performance achieved.

Acknowledgments

This research was sponsored by the General Dynamics Corporation with Jon Bohlmann and Mike Love serving as technical monitors. One of the authors was also sponsored by the National Science Foundation. Their support is greatly appreciated. The authors also acknowledge Douglas MacMartin for the asymptotic analysis (Eq. 8) and for his comments concerning the issues discussed in this paper.

References

[1]Horikawa, H., and Dowell, E. H., "An Elementary Explanation of the Flutter Mechanism with Active Feedback Controls," *Journal of Aircraft*, Vol. 16, No. 4, 1979, pp. 225–232.

[2]Ohta, H., Fujimori, A., Nikiforuk, P. N., and Gupta, M. M., "Active Flutter Suppression for Two-Dimensional Airfoils," *Journal of Guidance, Control, and Dynamics*, Vol. 12, No. 2, 1989, pp. 188–194.

[3]Mahesh, J. K., Stone, C. R., Garrard, W. L., and Dunn, H. J., "Control Law Synthesis for Flutter Suppression Using Linear Quadratic Gaussian Theory," *Journal of Guidance and Control*, Vol. 4, No. 4, 1981, pp. 415–422.

[4]Newsom, J. R., Pototzky, A. S., and Abel, I., "Design of a Flutter Suppression System for an Experimental Drone Aircraft," *Journal of Aircraft*, Vol. 22, No. 5, 1985, pp. 380–386.

[5]Liebst, B. S., Garrard, W. L., and Adams, W. M., "Design of an Active Flutter Suppression System," *Journal of Guidance, Control, and Dynamics*, Vol. 9, No. 1, 1986, pp. 64–71.

[6]Karpel, M., "Design for Active Flutter Suppression and Gust Alleviation Using State-Space Aeroelastic Modeling," *Journal of Aircraft*, Vol. 19, No. 3, 1982, pp. 221–227.

[7]Mukhopadhyay, V., Newsom, J. R., and Abel, I., "Reduced-Order Optimal Feedback Control Law Synthesis for Flutter Suppression," *Journal of Guidance and Control*, Vol. 5, No. 4, 1982, pp. 389–395.

[8]Tiffany, S. H., and Karpel, M., "Aeroservoelastic Modeling and Applications Using Minimum-State Approximations of the Unsteady Aerodynamics," AIAA Paper 89-1188, April 1989.

[9]Perry, B., III, Mukhopadhyay, V., Hoadley, S. T., et al., "Digital-Flutter-Suppression-System Investigations for the Active Flexible Wing Wind-Tunnel Model," AIAA Paper 90-1074, May 1990.

[10]Zeiler, T. A., and Weisshaar, T. A., "Integrated Aeroservoelastic Tailoring of Lifting Surfaces," *Journal of Aircraft*, Vol. 25, No. 1, 1988, pp. 76–83.

[11]Crawley, E. F., and Lazarus, K. B., "Induced Strain Actuation of Isotropic and Anisotropic Plates," *AIAA Journal*, Vol. 29, No. 6, 1991, pp. 944–951.

[12]Ehlers, S. M., and Weisshaar, T. A., "Static Aeroelastic Behavior of an Adaptive Laminated Piezoelectric Composite Wing," AIAA Paper 90-1078, May 1990.

[13]Lazarus, K. B., Crawley, E. F., and Bohlmann, J. D., "Static Aeroelastic Control Using Strain Actuated Adaptive Structures," *Journal of Intelligent Materials Systems and Structures*, Vol. 2, No. 3, 1991, pp. 386–410.

[14]Bisplinghoff, R. L., Ashley, H., and Halfman, R. L., *Aeroelasticity*, Addison-Wesley, Reading, MA, 1955.

[15]Theodorsen, T., and Garrick, I. E., "Nonstationary Flow About a Wing-Aileron-Tab Combination Including Aerodynamic Balance," NACA Rept. 736, 1942.

[16]Lin, C. Y., and Crawley, E. F., "Strain Actuated Aeroelastic Control," Space Engineering Research Center, Rept. 2-93, Cambridge, MA, Feb. 1993.

[17]Crawley, E. F., and de Luis, J., "Use of Piezoelectric Actuators as Elements of Intelligent Structures," *AIAA Journal*, Vol. 25, No. 10, 1987, pp. 1373–1385.

[18]Fleming, F. M., and Crawley, E. F., "The Zeros of Controlled Structures: Sensor/Actuator Attributes and Structural Modelling," AIAA Paper 91-0984, April 1991.

[19]Freudenberg, J. S., and Looze, D. P., "Right Half Plane Poles and Zeros and Design Tradeoffs in Feedback Systems," *IEEE Transactions on Automatic Control*, Vol. AC-30, No. 6, 1985, pp. 555–565.

[20]Miller, D. W., Jacques, R. N., and de Luis, J., "Typical Section Problems for Structural Control Applications," AIAA Paper 90-1225, April 1990.

[21]Emami-Naeini, A., and Rock, S. M., "On Asymptotic Behavior of Non-Square Linear Optimal Regulators," *Proceedings of the 23rd Conference on Decision and Control* (Las Vegas, NV), IEEE, 1984, pp. 1762, 1763.

[22]Pan, W., Zhang, Q., Bhalla, A., and Cross, L. E., "Field-Forced Antiferroelectric-to-Ferroelectric Switching in Modified Lead Zirconate Titanate Stannate Ceramics," *Journal of the American Ceramic Society*, Vol. 72, No. 4, 1989, pp. 571–578.

[23]Kwakernaak, H., and Sivan, R., "The Maximally Achievable Accuracy of Linear Optimal Regulators and Linear Optimal Filters," *IEEE Transactions on Automatic Control*, Vol. AC-17, No. 1, 1972, pp. 79–86.

[24]Nissim, E., "Flutter Suppression Using Active Controls Based on the Concept of Aerodynamic Energy," NASA TN D-6199, 1971.